JOURNAL OF MATERIALS SCIENCE 28 (1993) 5975–5980

Nitriding behaviour in Fe–Al–Mn–Cr–C alloys at 1000–1100 °C

J. G. DUH, S. C. LIN
Department of Materials Science and Engineering, National Tsing Hua University, Hsinchu, Taiwan 300

Nitridation in alloys with compositions Fe–31Mn–9Al–0.87C–xCr ($x = 0$, 3, 6) was investigated. The alloy developed a needle-like nitriding product of AlN in a nitrogen atmosphere at 1000–1100 °C. The measured penetration depth and the evaluated nitriding rate increased with temperature and the chromium content in the alloy. A quasi-steady state diffusion model of nitrogen migration through the alloy has been employed to describe the kinetics of nitridation. The activation energy of the nitriding rate was also evaluated.

1. Introduction

In the past decade, a great deal of research activity has focused on the development of the potential Fe–Al–Mn-based alloy as a substitute for conventional Fe–Ni–Cr stainless steel. The high-temperature oxidation behaviour of this alloy system has been intensively investigated [1–14]. A series of work has been carried out continuously by our research group concerning the high-temperature behaviour of Fe–Al–Mn-based alloys, including the elemental distribution and formation morphology in the oxidation layer [7, 9, 11, 13, 14], the effect of gaseous atmosphere and pretreatment [10], the development of the oxidation-induced ferrite layer [12], and the proposed diffusion-related mechanism in the oxidation-induced phase transformation [15]. In addition to the oxidation behaviour mentioned above, a nitriding phenomenon was observed in Fe–31Mn–9Al–6Cr–0.86C alloy oxidized in dry air at temperatures above 800 °C [16]. A needle-like nitriding product of AlN developed towards the alloy matrix. It was argued that the degree of solubility of nitrogen played a major role in the nitriding.

Recently, the nitriding kinetics of Fe–Al–Mn–Cr–C alloys at 1000 °C was investigated [17]. The purpose of the present research was to study the nitriding behaviour of Fe–Al–Mn-based alloy at various temperatures. The thickness of the nitriding layer was measured as a function of the oxidation time and employed to evaluate the nitriding rate of the Fe–Al–Mn alloy.

2. Experimental procedure

The alloys with different compositions were prepared from electrolytic iron (99%), electrolytic manganese (99.96%) electrolytic chromium (99.92%) and high-purity aluminium (99.99%) in a Leybold-Heraeus IS 8/III vacuum melting furnace. Iron, aluminium and chromium were first loaded at about 10^{-2} mbar. Manganese and carbon were then charged at the end of the melting process by introducing argon gas into the chamber to reduce the loss of manganese and carbon due to evaporation. After melting, casting was performed into a steel mould at about 1600 °C. The compositions of the alloys were analysed by wet chemical analysis and are listed in Table I.

The as-fabricated ingots were forged at 1200 °C with 75% reduction and then homogenized at 1200 °C for 11 h. After surface finishing, the alloys were hot rolled with 90% reduction to a thickness of 2.3 mm. The alloys were subsequently surface finished to avoid the impurities diffusing into the alloy during the annealing process, which was carried out at 1150 °C for 50 h in a quartz tube with flowing argon. The alloys were cut into pieces with the dimensions of 10 mm $\times$ 10 mm $\times$ 2 mm. The specimen was abraded up to 1200 grit SiC paper, polished up to 0.05 μm aluminium oxide powder, ultrasonically degreased in acetone and then rinsed in alcohol.

The polished specimen was first put into a specially designed stainless steel (AISI-310) tube. Prior to nitridation, the stainless steel tube was first purged with nitrogen and then evacuated by the mechanical pump to 30 mtorr. The outgassing was repeated three times to eliminate any other gas species besides nitrogen. The nitriding experiment was carried out at 1000°, 1050° and 1100 °C, with dried nitrogen at a flow rate of 120 $cm^3\,min^{-1}$. The constant temperature zone within the variation $\pm$ 1 °C, inside the furnace was about 8 cm. The inlet nitrogen was dried through a calcium chloride drying tube before entering the furnace. The nitridation time for each alloy was 1, 2, 4, 8, 12, 18 and 24 h at each temperature. To freeze the high-temperature structure, all specimens were water quenched after nitridation. Two specimens with the identical composition were nitrided under the same condition. One was employed for the X-ray diffraction study and another for electron microprobe analysis and optical observation. The latter one was cold mounted, and cut to reveal the cross-section with a low-speed diamond saw. Specimens were then ground

0022–2461

TABLE I Chemical compositions (wt %) of the alloys employed in this study

Alloy	Mn	Al	Cr	C	Fe
A	31.18	8.96	–	0.87	Bal.
B	30.95	8.87	2.98	0.87	Bal.
C	31.30	8.92	5.96	0.86	Bal.

and polished up to 0.05 μm aluminium oxide powder, and etched for 10–15 s with 10% Nital etching solution.

The possible phases present in given conditions, i.e. various compositions, nitridation times and temperatures, were identified with a Rigaku X-ray diffractometer equipped with copper target, nickel filter and graphite single-crystal monochrometer. The morphology of the nitrided layer and the penetration depth of the nitrided layer were examined by both optical microscopy (OM) and scanning electron microscopy (SEM). The elemental redistribution after nitridation was detected through X-ray microanalysis technique with an electron microprobe (Jeol JCXA-733).

3. Results and discussion

After homogenization annealing, austenite is the only phase observed on the basis of the X-ray diffraction data for Alloys A, B and C. By comparing with nitrided specimen, it appears that no evident grain growth occurred during the nitridation [18].

The structure of the nitrided specimen was determined with the X-ray diffractometer operated at 45 kV and 20 mA with a scanning speed of $2\,^{\circ}C\,min^{-1}$. From the X-ray diffraction pattern as shown in Fig. 1 for Alloy A nitrided at 1000 °C for 24 h, nitride AlN is formed in addition to the original phase. The microstructure of Alloy A nitrided at 1000 °C for 24 h is shown in Fig. 2. The morphologies of Alloys A, B and C after nitridation are similar. A region containing needle-like structure is observed beneath the free surface of the alloy. The needle-like structure is identified as AlN on the basis of X-ray diffraction results, as indicated in Fig. 1. Further identification can be made with the aid of X-ray mapping technique of electron microprobe analysis. A typical scanning electron micrograph of the nitriding structure formed on alloys is shown in Fig. 3a. The X-ray mapping for each element is presented in Fig. 3b–e. It is apparent that the nitrided structure is rich in aluminium, but depleted in iron, manganese and chromium. As nitriding occurs and results in AlN, the aluminium content is depleted between the needle-like structure. A quantitative analysis with the aid of electron microprobe indicates that the aluminium content between the AlN plates is only 0.08 wt % [17]. The penetration depths of the nitriding layer for alloys with different times at 1000, 1050 and 1100 °C are given in Tables II, III and IV, respectively. It appears that the depth of the nitriding layer increases with time. The penetration depth of the nitriding layer at a given time and fixed temperature in Alloy C is the largest, followed by that in Alloy B and it is the least in Alloy A. The corresponding plots of thickness of the nitriding layer versus the square root of time on the basis of Tables II, III, and IV are presented in Figs 4–6 for Alloys A, B and C, respectively. It is apparent that the nitriding layer grows parabolically with time. According to the parabolic rate law formulation

$$\xi = (K_N t)^{1/2} \quad (1)$$

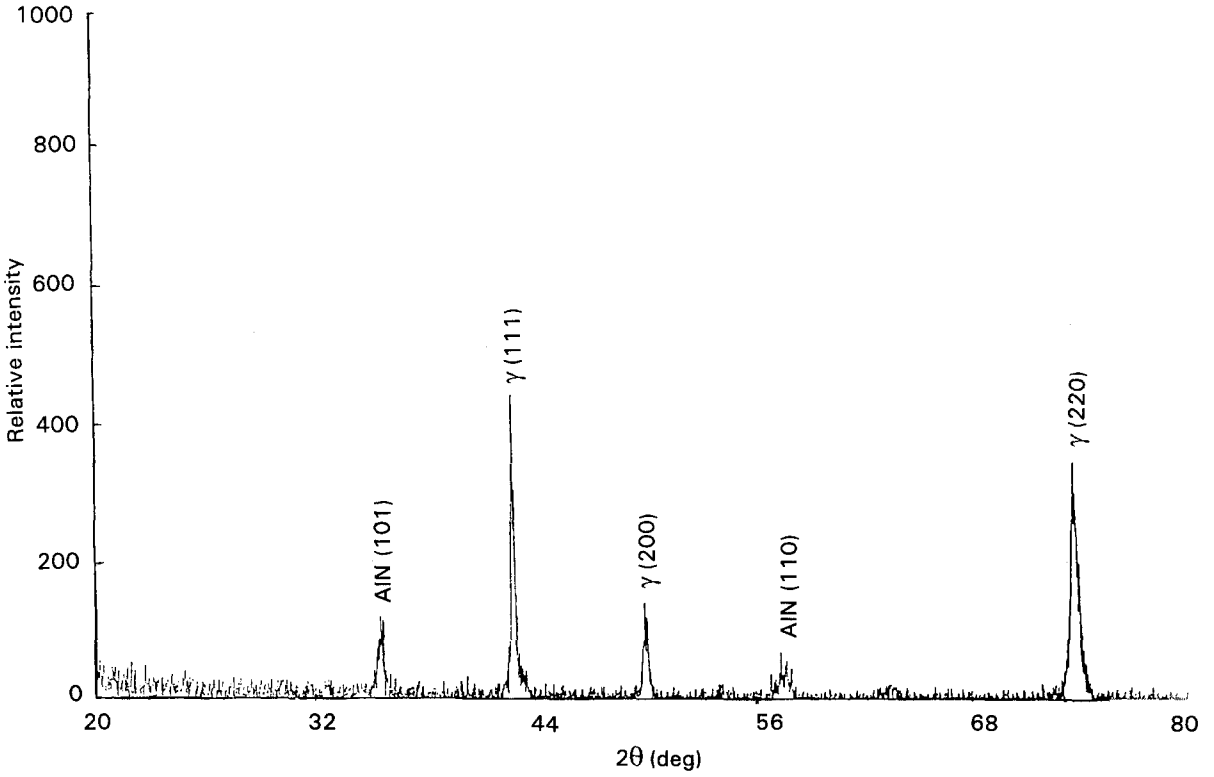

Figure 1 X-ray diffraction pattern of Alloy A nitrided at 1000 °C for 24 h. AlN nitride phase is present.

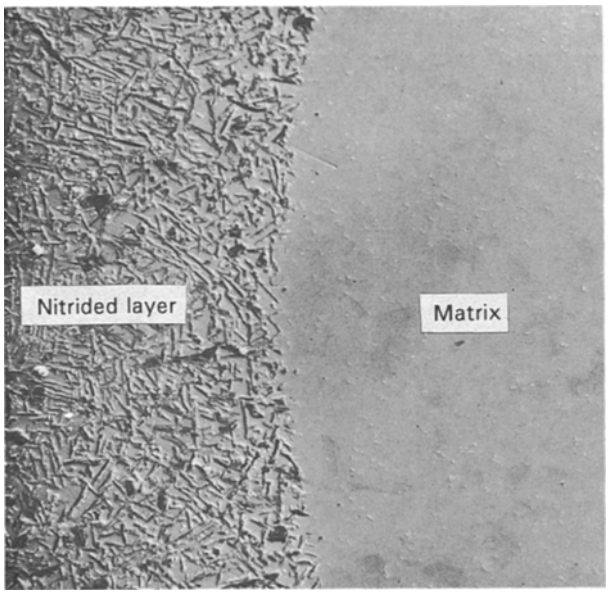

Figure 2 Scanning electron micrograph of the nitriding layer formed on Alloy A at 1000 °C for 24 h.

where ξ is the thickness of the nitriding layer, K_N the nitriding rate, and t is the nitriding time. The nitriding rates, K_N, for Alloys A, B and C at various temperatures have been evaluated according to Equation 1 and are summarized in Table V. The physical implication underlying the nitriding rate will be discussed from the viewpoint of diffusional transport.

In the austenitic structure of Fe–Mn–Al–Cr alloy, nitrogen is located in the interstitial site, while aluminium is in the substitutional lattice. In general, the diffusivity of the interstitial nitrogen is greater than that of the substitutional aluminium because of the atomic size effect. As a result, the nitriding behaviour in Fe–Mn–Al–Cr alloy can be considered to be another type of internal oxidation according to Wagner's formulation [19]. The internal nitriding migrates through the inward diffusion of nitrogen, and aluminium in the internal matrix is presumed to be nitrided immediately on the spot. Therefore, the rate of nitriding can be derived for a planar specimen geometry by the quasi-steady-state approximation. Consider a planar specimen of a multicomponent alloy. Assume the ambient nitrogen partial pressure is sufficient to nitride one of the constituent elements, say aluminium in Fe–Al–Mn–Cr–C alloy. The quasi-steady-state approximation assumes the dissolved nitrogen concentration varies linearly across the zone of internal nitriding [20]. From Fick's law and the consideration of the reaction of nitrogen with aluminium, one could derive the penetration depth of the nitriding layer at time, t, as follows [17]

$$\xi = \left[\frac{2N_N^{(s)} D_N}{N_{Al}^{(o)}} t\right]^{1/2} \quad (2)$$

where D_N is the diffusivity of nitrogen in the alloy system, $N_N^{(s)}$ is the nitrogen solubility, and $N_{Al}^{(o)}$ is the molar fraction of aluminium in the matrix. For the alloys employed in this study, the molar fraction of aluminium is around 16% from the compositions as listed in Table I. Thus, Equation 2 takes the form

$$\xi = [12.5 N_N^{(s)} D_N t]^{1/2} \quad (3)$$

TABLE II The penetration depth of the nitriding layer at 1000 °C for Alloys A, B and C

	Penetration depth (μm)						
	1h	2h	4h	8h	12h	18h	24h
Alloy A	54.7 ± 16.8	86.2 ± 10.4	116.9 ± 18.9	175.5 ± 12.1	209.4 ± 15.9	261.8 ± 16.5	298.9 ± 17.6
Alloy B	68.4 ± 12.4	109.6 ± 21.3	156.4 ± 18.1	219.8 ± 13.5	275.9 ± 25.3	326.8 ± 15.3	377.8 ± 22.7
Alloy C	100.1 ± 12.5	146.6 ± 18.7	188.9 ± 19.5	284.1 ± 19.5	365.2 ± 16.8	428.3 ± 19.6	498.5 ± 28.2

TABLE III The penetration depth of the nitriding layer at 1050 °C for Alloys A, B and C

	Penetration depth (μm)						
	1h	2h	4h	8h	12h	18h	24h
Alloy A	66.1 ± 12.8	99.8 ± 13.5	138.9 ± 13.2	204.6 ± 18.9	244.5 ± 23.9	308.7 ± 25.3	352.1 ± 19.4
Alloy B	81.7 ± 13.3	113.7 ± 15.7	173.6 ± 16.9	248.0 ± 20.8	302.8 ± 28.3	366.4 ± 16.5	429.3 ± 21.7
Alloy C	102.6 ± 20.6	150.2 ± 22.2	219.6 ± 20.0	319.9 ± 16.7	381.1 ± 13.6	470.4 ± 11.2	547.0 ± 35.2

TABLE IV The penetration depth of the nitriding layer at 1100 °C for Alloys A, B and C

	Penetration depth (μm)						
	1h	2h	4h	8h	12h	18h	24h
Alloy A	88.2 ± 22.8	126.3 ± 18.9	188.6 ± 18.8	268.7 ± 13.2	315.4 ± 20.1	376.9 ± 22.5	434.4 ± 29.7
Alloy B	100.3 ± 18.9	147.8 ± 11.3	202.2 ± 14.4	297.6 ± 18.2	350.7 ± 22.7	425.2 ± 17.7	512.0 ± 33.7
Alloy C	112.3 ± 21.8	179.5 ± 16.4	258.1 ± 15.5	363.1 ± 22.3	440.9 ± 25.8	534.0 ± 20.1	620.1 ± 36.2

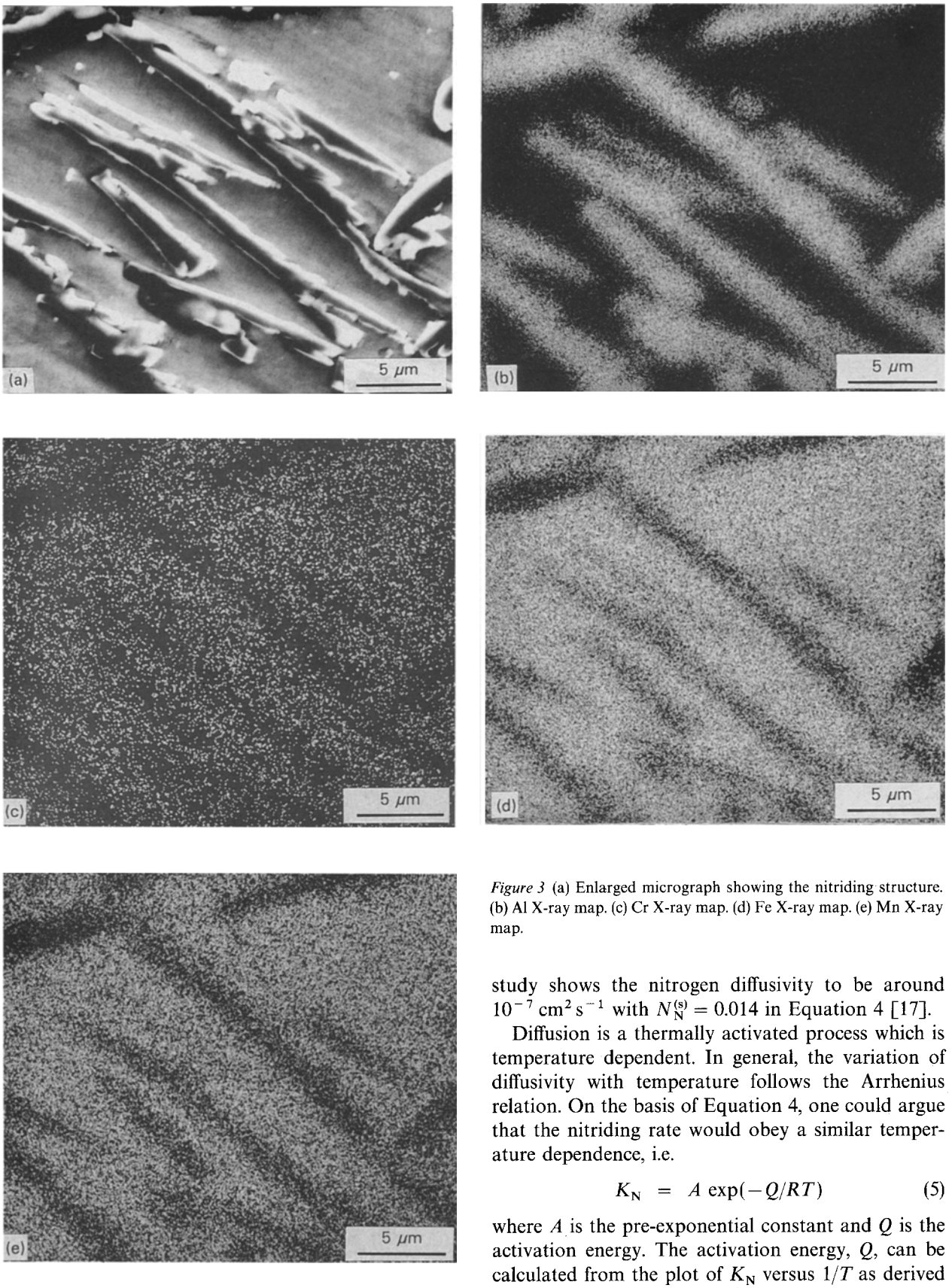

Figure 3 (a) Enlarged micrograph showing the nitriding structure. (b) Al X-ray map. (c) Cr X-ray map. (d) Fe X-ray map. (e) Mn X-ray map.

Comparing Equation 1 and 3, one obtains

$$K_N = 12.5 N_N^{(s)} D_N \quad (4)$$

Equation 4 implies that the nitriding rate is dependent on the diffusivity of nitrogen, as well as the solubility of nitrogen in the alloy system. In principle, Equation 4 provides the evaluation of nitrogen diffusivity if the solubility data is known. A preliminary study shows the nitrogen diffusivity to be around 10^{-7} cm^2 s^{-1} with $N_N^{(s)} = 0.014$ in Equation 4 [17].

Diffusion is a thermally activated process which is temperature dependent. In general, the variation of diffusivity with temperature follows the Arrhenius relation. On the basis of Equation 4, one could argue that the nitriding rate would obey a similar temperature dependence, i.e.

$$K_N = A \exp(-Q/RT) \quad (5)$$

where A is the pre-exponential constant and Q is the activation energy. The activation energy, Q, can be calculated from the plot of K_N versus $1/T$ as derived on the basis of Table V. Table VI summarizes the evaluated nitriding free energy and nitriding constant for Alloys A, B and C.

It should be pointed out that no nitrogen solubility data are available in the literature for Fe–Al–Mn-based alloy. Grabke reported the nitrogen solubility in Fe–28.6 at % Mn at 1000 °C in 0.95 atm N_2 to be around 1.49 at % [21]. Substituting $N_N^{(s)} = 0.0149$ into Equation 4, a value of $D_N = 1.24 \times 10^{-7}$ cm^2 s^{-1} is obtained for Alloy A at 1100 °C, which is close to the

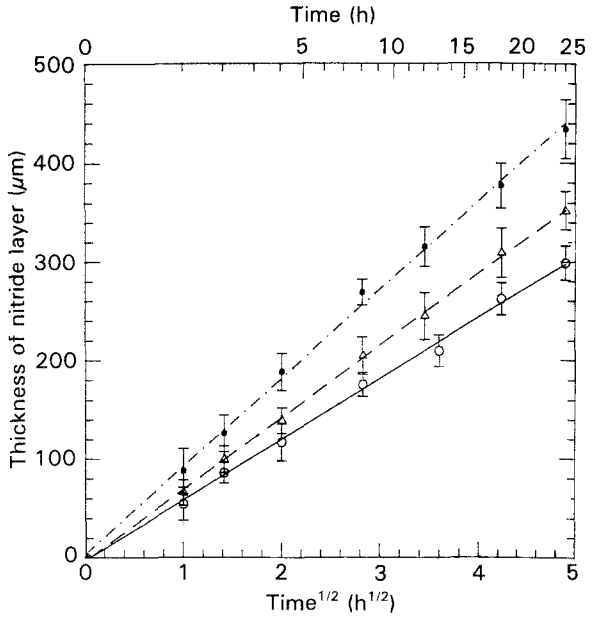

Figure 4 The penetration depth of the nitrided layer as a function of time for Alloy A at (○) 1000 °C, (△) 1050 °C, (●) 1100 °C.

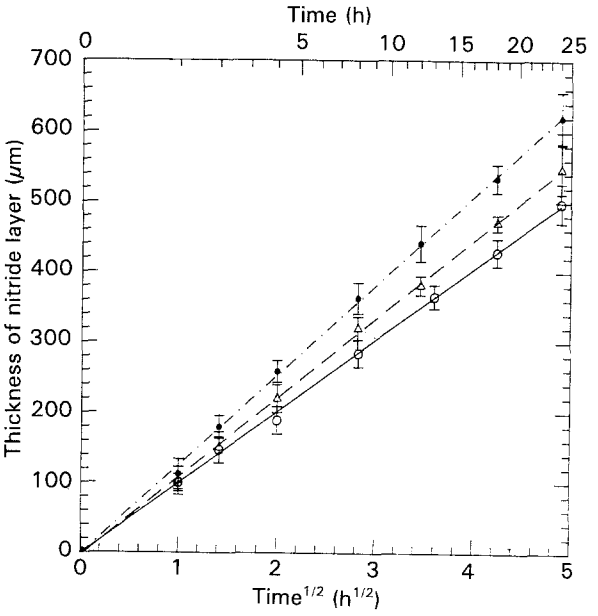

Figure 6 The penetration depth of the nitrided layer as a function of time for Alloy C at (○) 1000 °C, (△) 1050 °C, (●) 1100 °C.

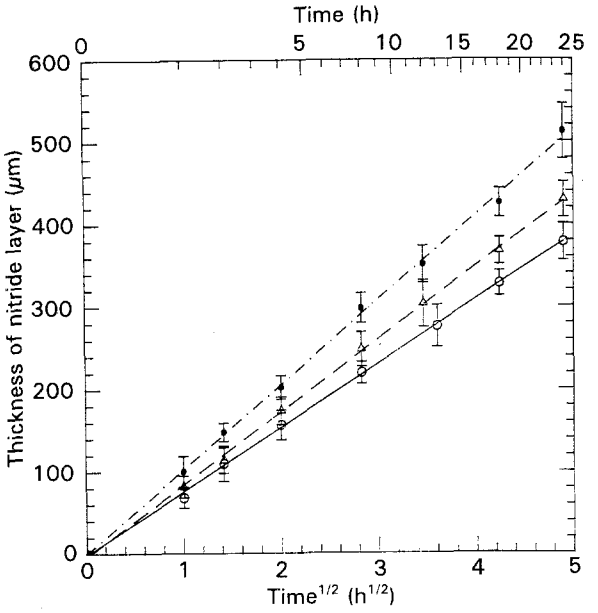

Figure 5 The penetration depth of the nitrided layer as a function of time for Alloy B at (○) 1000 °C, (△) 1050 °C, (●) 1100 °C.

TABLE V The calculated nitriding rate for Alloys A, B and C at various temperatures

	Nitriding rate (10^{-8} cm^2 s^{-1})		
	1000 °C	1050 °C	1100 °C
Alloy A	1.1 ± 0.1	1.4 ± 0.2	2.3 ± 0.2
Alloy B	1.7 ± 0.1	2.0 ± 0.2	2.9 ± 0.2
Alloy C	2.9 ± 0.1	3.3 ± 0.2	4.4 ± 0.3

TABLE VI The calculated nitriding free energy and constant for Alloys A, B and C

Alloy	Nitriding constant (cm^2 s^{-1})	Nitriding free energy (kcal mol^{-1})
A	(3.0–0.2) ± 10^{-4}	26.0
B	(2.7–0.2) ± 10^{-5}	18.7
C	(1.2–0.1) ± 10^{-5}	15.4

TABLE VII Activation energy of nitrogen diffusion in alloys

Alloy	Activation energy (kcal mol^{-1})	Reference
FeCr	41.5–43.3	[22]
CrTi	24 –28	[23]
Fe–Al–Mn–Cr	15 –26	This study

diffusion of nitrogen in Fe–2.82Cr–0.01N alloys at 1100 °C where $D_N = 1.65 \times 10^{-7}$ cm^2 s^{-1} [22]. Arnold and Hagel [23] also reported similar nitrogen diffusivity $(1.29–1.89) \times 10^{-7}$ cm^2 s^{-1} for Cr–Ti alloys at 1000 °C. However, the nitriding rate of Cr_2N in Cr–Ti alloys around $(5–6.8) \times 10^{-10}$ cm^2 s^{-1} is two orders of magnitude smaller than that in Fe–Al–Mn alloy in this study. This indicates that the solubility of nitrogen, instead of the nitrogen diffusivity, should play a major role in the nitriding behaviour of the alloy system. For the sake of comparison, it might be worthwhile to note that the calculated activation energy of nitriding rate in Fe–Al–Mn alloys is much smaller than the activation energy of nitrogen diffusion in FeCr alloy in which Q ranges from 41.5–43.3 kcal mol^{-1} [22]. In addition, the activation energy of nitrogen diffusion in CrTi alloys is around 24–28 kcal mol^{-1} [23], which is somewhat larger than those in this study, i.e. 15–26 kcal mol^{-1}. The tabulation of the activation energy of nitrogen diffusion in various alloy systems is summarized in Table VII.

It is worthwhile to point out that K_N in Equation 1 should reflect changes in $N_N^{(s)}$ and D_N with temperature, as indicated in Equation 4 and the combined temperature effect should be attainable from an Arrhenius plot. However, one should also realize that

this is a combined effect. In this study, the combined temperature effect is represented by the measurable nitriding rate. One might also argue that the changes in K_N reflects the changes in reciprocal of N^{o}_{Al} at each temperature. Nevertheless, in the fabrication of alloys, we intentionally made a nearly isoconcentration of aluminium in every Fe–Al–Mn system. The way we treated the problem was to assume a constant value for N_{Al} and thus reach the conclusion in Equations 3 and 4. In fact, one should realize that the overall nitriding behaviour is a combined effect due to changes in $N^{(s)}_N$, D_N and $N^{(o)}_{Al}$, as revealed in Equation 2. $N^{(o)}_{Al}$ could be attainable from the experimental data, while $N^{(s)}_N$ and D_N are not available in this new alloy system. It is a challenge to separate the combined effect of $N^{(s)}_N$ and D_N, if more experimental data are available in the Fe–Al–Mn system.

The solubility of the solute element, in fact, depends upon the phase of microstructure in the alloy system. Generally speaking, the solubility of nitrogen in the ferrite phase is smaller than that in the austenitic phase. Thus the growth of AlN prevails in the austenitic region instead of the ferrite, which is consistent with the previous observation [16]. It is also observed that the nitriding rate in this study increases as the chromium content increases, as shown in Table V. Grabke *et al.* [21] proposed that the chromium addition in the Fe–Mn system would increase the solubility of nitrogen in the alloy. Because the atomic sizes of chromium and manganese are larger than that of iron, the addition of chromium enlarges the lattice parameter [17] and consequently increases the interstitial site spacing, which in turn enhances the nitrogen content in the interstitialcy. Hence, the nitriding rate enhanced for the alloy with a greater chromium content.

4. Conclusions

1. Alloys with compositions Fe–31Mn–9Al–0.87C–xCr ($x = 0$, 3 and 6) develop a needle-like nitriding product of AlN in a nitrogen atmosphere at 1000–1100 °C.

2. The reaction front of the nitriding layer migrates parabolically with time. The measured penetration depth and the evaluated nitriding rate increases with temperature and the chromium content in the alloy.

3. The kinetics of nitriding is presented with a quasi-steady-state diffusion model of nitrogen migration through the alloy. The nitriding rate depends on the solubility of nitrogen and the diffusivity of nitrogen in the alloy system.

4. Activation energy of the nitriding rate, Q, is evaluated according to the Arrhenius relation, which is in the order of 20 kcal mol^{-1} for the alloys employed in this study.

5. The solubility of nitrogen is the dominating factor in the nitriding behaviour of Fe–Al–Mn alloy, and addition of chromium into Fe–Al–Mn alloy enhances the nitriding rate.

Acknowledgement

The authors thank the National Science Council, Taiwan, for financial support under contract NSC78-0405-E007-12.

References

1. S. K. BANERJI, in "Workshop on Trends in Critical Materials Requirements for Steels of the Future-Conservation and Substitution Technology for Chromium", Vanderbilt University, Nashville, Tennessee, October, 1982.
2. J. P. SAUER, R. A. RAPP and J. P. HIRTH, *Oxid. Metals* **18** (1982) 285.
3. P. TOMASZEWICZ and G. R. WALLWORK, *ibid.* **20** (1983) 75.
4. P. R. S. JACKSON and G. R. WALLWORK, *ibid.* **21** (1984) 135.
5. *Idem, ibid.* **20** (1983) 1.
6. R. WANG, M. J. STRASZHEIM and R. A. RAPP, *ibid.* **21** (1984) 71.
7. J. G. DUH, C. J. LIN, J. W. LEE and C. M. WAN, in "Proceedings of Alternate Alloying for Environmental Resistance", edited by G. R. Smolik and S. K. Banerji (The Metallurgical Society, Warrendale, Pennsylvania, PA, 1987) p. 283.
8. C. H. KAO, C. M. WAN and M. J. JAHN, *ibid.*, p. 347.
9. J. G. DUH, C. J. WANG, C. M. WAN and B. S. CHIOU, *ibid.*, p. 291.
10. C. J. WANG and J. G. DUH, *J. Mater. Sci.* **23** (1988) 2913.
11. *Idem, ibid.* **23** (1988) 3447.
12. J. G. DUH, J. W. LEE and C. J. WANG, *ibid.* **23** (1988) 2649.
13. J. G. DUH and C. J. WANG, *ibid.* **25** (1990) 268.
14. *Idem, ibid.* **25** (1990) 2063.
15. J. G. DUH and J. W. LEE, *J. Electrochem. Soc.* **136** (1989) 847.
16. C. J. WANG and J. G. DUH, *J. Mater. Sci.* **23** (1988) 769.
17. J. G. DUH and C. J. WANG, *ibid.* **25** (1990) 2615.
18. S. C. LIN, MS thesis, National Tsing Hua University, Hsinchu, Taiwan (1990).
19. C. WAGNER, *J. Electrochem. Soc.* **63** (1959) 777.
20. N. BIRKS and G. H. MEIER, in "Introduction to High Temperature Oxidation of Metals" (Edward Arnold, London, 1983) p. 95.
21. H. J. GRABKE, SK. IYER and S. K. SRINIVASAN, *Z. Metallkde* **66** (1975) 286.
22. E. ICHISE, R. YAMABA and T. MORI, *Suppl. Trans. Iron Steel Inst. Jpn* **11** (1971) 535.
23. J. L. ARNOLD and W. C. HAGEL, *Metall. Trans.* **3** (1972) 1471.

Received 19 February 1992
and accepted 28 April 1993